Magnetic structures in ordered and disordered γ-FeMn alloys: Ordering due to disorder

D. Spišák and J. Hafner
Institut für Materialphysik and Center for Computational Materials Science, Universität Wien, Sensengasse 8/12, A-1090 Wien, Austria
(Received 16 November 1999)

We present calculations of the magnetic properties of ordered and disordered γ-FeMn using a self-consistent tight-binding linearized muffin-tin orbital approach allowing for noncollinear spin structures. In an ordered compound $Fe_{0.5}Mn_{0.5}$ we find a ground state with parallel Fe moments and canted Mn moments forming an angle of 128°. If substitutional disorder is present in the system, a uniform collinear antiferromagnetic order builds up. A possible explanation of this result is proposed.

I. INTRODUCTION

γ-FeMn alloys with a face-centered-cubic (fcc) structure have been investigated for a long time mainly as a system from which the magnetic properties of pure, at room temperature unstable, fcc-Fe and fcc-Mn (γ-Fe and γ-Mn) could be extrapolated. Because FeMn alloys do not form any intermetallic compound, they can be studied over a wide range of temperature and composition. In an early paper[1] a long-range antiferromagnetic (AFM) order in γ-FeMn was detected and two alternative magnetic structures were suggested, which conform to the neutron-diffraction data for polycrystals, but cannot be discriminated—a collinear type-I AFM configuration [cf. Fig. 1(a)] and a configuration with unit cell of four atoms with the magnetic moments pointing towards the cell center, i.e., along $\langle 111 \rangle$ directions [cf. Fig. 1(e)]. It was concluded that the nearest-neighbor interactions between Mn-Mn and Mn-Fe atoms are antiferromagnetic and that the Fe-Fe interactions cannot be strongly ferromagnetic (FM). On the basis of Mössbauer and neutron-diffraction measurements the magnetic phase diagram of γ-Fe_xMn_{1-x} was constructed,[2] with three different types of antiferromagnetic structures. At the Mn-rich end with $x \leqslant 0.3$ a γ-Mn-like collinear AFM structure is stabilized, at the Fe-rich end ($x \geqslant 0.8$) a γ-Fe-like AFM structure was found. In the intermediate region a distinctly different noncollinear ordering should develop with a remarkable change of the Néel temperature and the average magnetic moment in opposite directions. The magnetic moment reaches its minimum of about $1\mu_B$ at the equiatomic composition, while the Néel temperature a maximal value of 520 K at that composition. Somewhat larger estimates of the average zero-temperature magnetic moments of $\langle m \rangle = 1.2 \pm 0.2\mu_B$, $|m_{Mn} - m_{Fe}| = 0.3 \pm 0.3\mu_B$ were reported by Ishikawa and Endoh.[3] It is to be noted, however, that quite different magnetic moments may reside on Fe and Mn atoms, since the hyperfine field acting on the Fe nuclei is much smaller that expected from the average moment and the temperature and composition dependences of the Fe and Mn moments are substantially different.[3,4] These facts contradict the picture of a uniform spin structure supported also by the absence of a broadening of the magnetic diffraction peaks typical for random alloys.[4] The spin-wave spectra obtained by inelastic neutron scattering were attributed either to a collinear type-I AFM structure,[5] or to the itinerant rather than localized character of magnetic moments.[6] However, in the latter study only nearest and next-nearest interactions in the localized model were taken into account and it was concluded that the short-range interaction cannot explain the measured isotropic spin dispersion relation.

In order to understand the complex magnetic behavior of γ-FeMn alloys several theoretical studies were performed.[7–11] Most of them considered an ordered γ-FeMn intermetallic compound with a cubic unit cell of the AuCu-I type with four atoms in the basis. The investigation of the volume dependence of the magnetic properties of collinear γ-FeMn revealed that the ground state within the local spin-density (LSD) approximation is a phase with nonzero AFM Mn moments and no Fe moments, with a lattice constant 3.1% smaller than the experimental value.[7] Interestingly, at a larger volume a different equilibrium magnetic structure with nonzero FM Fe moments and larger ferrimagnetic Mn moments forms. Fe moments are formed at densities about halfway between the theoretical LSD-equilibrium density and the experimental density. Hence the failure to predict the formation of Fe moments in γ-FeMn is directly related to the overbinding characteristic of the LSD approximation. We should also note that the LSD approximation fails to predict the correct magnetic ground state for both Fe (Ref. 12) and Mn.[13,14] The LSD-approximation ground state of Fe is nonmagnetic hcp, for γ-Mn nonmagnetic AFM and FM states are energetically almost degenerate. Generalized gradient corrections to the LSD approximation favor the magnetic over the nonmagnetic states and lead to an expansion of the magnetic phases (large magneto volume effect).[12–14] First total-energy calculations allowing for a noncollinear spin arrangement were performed by Kübler *et al.*[8] They found a noncollinear ground state with large moments ($m_{Fe} = 1.41\mu_B$, $m_{Mn} = 2.05\mu_B$, but the collinear AFM configuration lies only 0.25 mRy/atom higher in energy. The drawback of their approach is the inclusion of only the spin-independent part of the effective potential in the Schrödinger equation. Similar self-consistent calculations for several possible collinear and noncollinear spin orderings carried out by Fujii *et al.*[9] predict the spin structure shown in Fig. 1(d) as the most stable one. Again the Mn moments were predicted to be substantially larger than the Fe moments. Effects of the substitutional disorder on the magnetic properties of γ-$Fe_{50}Mn_{50}$ were investigated in the first-principle calculations by Johnson *et al.*[10] using the Korringa-Kohn-Rostocker

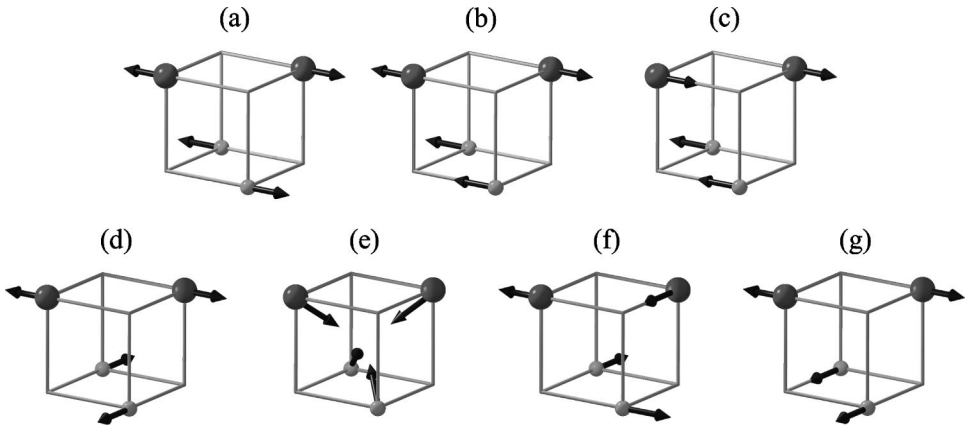

FIG. 1. Spin configurations considered in the calculations for ordered γ-FeMn. Smaller spheres denote Fe atoms, larger spheres represent Mn atoms.

coherent-potential approximation (KKR-CPA). The calculated magnetic moments on the Fe and Mn sites are antiparallel, namely $m_{Fe}=1.64\mu_B$ and $m_{Mn}=-1.04\mu_B$. Note the inversion of the magnitudes of magnetic moments compared to the results for the ordered compounds. It was also inferred that some unspecified type of ordered AFM state could not be ruled out. Recently the variation of the magnetic moments as a function of composition in disordered fcc and bcc Fe_xMn_{1-x} was studied by Kulikov and Demangeat[11] within KKR-CPA. Most surprising result was the existence of a stable solution with vanishing Fe and Mn moments near the equiatomic concentration. The conclusion is that evidently the disorder has a strong influence on the magnetic ground state. However, the prediction of Mn moments that are substantially smaller than the average Fe moments, or of an almost complete quenching leading to the conclusion that single-site theories do not yield a correct description of magnetism in concentrated Fe_xMn_{1-x} alloys.

In this paper we address the issue of the true ground state of ordered γ-FeMn compound within LSD and gradient corrected LSD approximations without any constraint on magnitude or direction of the magnetic moments. To compare our results with the previous conclusions, a few magnetic structures with the orientation of the magnetic moments kept fixed during self-consistent calculation are included. Besides, the variation of the magnetic moments and the total energy with the angle between the Mn and Fe moments and relative to some chosen axes was explored. The effect of disorder on the magnetic structure was studied and discussed.

II. COMPUTATIONAL DETAILS

The extension of density-functional theory to a treatment of noncollinear magnetic structure was formulated by Kübler *et al.*,[8,15] where the details related to the implementation in the augmented spherical-wave method were given as well. This formalism was used by several groups to allow for noncollinearity within the linearized muffin-tin orbital (LMTO) method[9,16–18] and plane-wave code.[19]

Here we shall shortly outline our approach to self-consistent electronic structure calculations for systems with noncollinear magnetic moments. It is based on the two-center tight-binding LMTO Hamiltonian

$$H_{\mathbf{R}L\alpha,\mathbf{R}'L'\beta}=C_{\mathbf{R}L\alpha}\delta_{\mathbf{R}\mathbf{R}'}\delta_{LL'}\delta_{\alpha\beta}+\sqrt{\Delta_{\mathbf{R}L\alpha}}S_{\mathbf{R}L,\mathbf{R}'L'}U_{\mathbf{R}\alpha,\mathbf{R}\gamma}U^{+}_{\mathbf{R}'\gamma,\mathbf{R}'\beta}\sqrt{\Delta_{\mathbf{R}'L'\beta}}, \tag{1}$$

expressed in terms of the structure constants S and the potential parameters of the LMTO method C, Δ which are evaluated in the nearly orthogonal representation.[20,21] The potential parameters depend on the solution of the radial Schrödinger equation at an arbitrary fixed energy, chosen in the energy region of interest. The label $\mathbf{R}$ denotes the atomic position, $L=(l,m)$ the angular momentum, and the greek letters spin indices. The matrix $U_{\mathbf{R}}$ signifies a (2×2) rotation matrix in a spin space,

$$U_{\mathbf{R}}(\varphi_{\mathbf{R}},\vartheta_{\mathbf{R}})=\begin{pmatrix}\cos\frac{\vartheta_{\mathbf{R}}}{2}\exp\left(\frac{\mathrm{i}}{2}\varphi_{\mathbf{R}}\right) & \sin\frac{\vartheta_{\mathbf{R}}}{2}\exp\left(-\frac{\mathrm{i}}{2}\varphi_{\mathbf{R}}\right)\\ -\sin\frac{\vartheta_{\mathbf{R}}}{2}\exp\left(\frac{\mathrm{i}}{2}\varphi_{\mathbf{R}}\right) & \cos\frac{\vartheta_{\mathbf{R}}}{2}\exp\left(-\frac{\mathrm{i}}{2}\varphi_{\mathbf{R}}\right)\end{pmatrix}, \tag{2}$$

that determines the transformation between a common global frame of reference and a local one with the spin-quantization axis defined by angles $\vartheta_{\mathbf{R}}$ and $\varphi_{\mathbf{R}}$ with respect to the global frame of reference. We adopt the conventional atomic sphere approximation (ASA) and the assumption that within each sphere the magnetization density field is collinear. Only if magnetic moments in all atomic spheres are collinear, the $U_{\mathbf{R}}$ reduce to unit matrices and because the structure constants are spin independent and the matrices of potential parameters are diagonal the Hamiltonian given by Eq. (1) becomes diagonal in the spin space.

Each step of a self-consistent calculation begins by setting up the Hamiltonian matrix given by Eq. (1) for an input distribution of magnetic moments. From the eigenvalues and eigenvectors of this Hamiltonian the matrix of spherically averaged local spin-polarized densities of states (DOS) $n^{(G)}_{\mathbf{R}L\alpha,\mathbf{R}L\beta}$ (generally nondiagonal in spin space) and the related integrals over the DOS matrix

$$q^{(G)}_{\mathbf{R}\alpha,\mathbf{R}\beta}=\sum_L\int^{E_F}n^{(G)}_{\mathbf{R}L\alpha,\mathbf{R}L\beta}(E)\,\mathrm{d}E \tag{3}$$

TABLE I. Total energies relative to the energy of spin configuration shown in Fig. 1(d) and magnitudes of magnetic moments on Fe and Mn sites for spin arrangements in Figs. 1(a)–1(g) and the ground state (h). For the configuration (b) both Mn moments are given. The results in parentheses are taken from Fujii *et al.* (Ref. 9). The results were obtained within LSD and LSD+GGC approximations.

	Configuration			Stability	ΔE (mRy/atom)		m_{Fe} (μ_B)		m_{Mn} (μ_B)	
	Fe-Fe	Mn-Mn	Fe-Mn		LDA	GGC	LDA	GGC	LDA	GGC
(a)	$\uparrow\downarrow$	$\uparrow\downarrow$	$\uparrow\uparrow$	stable	0.41	0.88	1.38	1.54	1.81	2.08
					(0.40)		(1.17)		(1.97)	
(b)	$\uparrow\uparrow$	$\uparrow\downarrow$	$\uparrow\uparrow$	stable	0.87	1.23	1.16	1.35	1.57/2.24	1.84/2.57
(c)	$\uparrow\uparrow$	$\uparrow\uparrow$	$\uparrow\downarrow$	stable	1.60	2.51	1.46	1.71	1.47	1.76
					(1.70)		(1.39)		(1.62)	
(d)	$\uparrow\downarrow$	$\uparrow\downarrow$	$\rightarrow\uparrow$	stable	0.00	0.00	1.55	1.74	1.89	2.17
					(0.00)		(1.23)		(1.99)	
(e)		noncoll.		unstable	0.10	0.08	1.65	1.85	1.81	2.12
					(0.35)		(1.34)		(1.91)	
(f)		noncoll.		stable	0.50	0.79	1.60	1.79	1.71	2.01
					(0.62)		(1.38)		(1.85)	
(g)	$\uparrow\uparrow$	$\uparrow\downarrow$	$\rightarrow\uparrow$	unstable	0.46	0.35	1.21	1.46	2.04	2.38
(h)		noncoll.		stable	−0.84	−0.94	1.42	1.60	2.06	2.37

are computed. The superscript (G) indicates the global reference system. There is always a similarity transformation which diagonalizes $q^{(G)}_{\mathbf{R}\alpha,\mathbf{R}\beta}$ at each site $\mathbf{R}$,

$$\sum_{\gamma,\delta} U_{\mathbf{R}\alpha,\mathbf{R}\gamma} q^{(G)}_{\mathbf{R}\gamma,\mathbf{R}\delta} U^{+}_{\mathbf{R}\delta,\mathbf{R}\beta} = q^{(L)}_{\mathbf{R}\alpha,\mathbf{R}\beta}\delta_{\alpha\beta}. \tag{4}$$

Here $q^{(L)}_{\mathbf{R}\alpha,\mathbf{R}\alpha}$ is the total number of valence electrons with up ($\alpha=1$) and down ($\alpha=2$) spins with respect to a local frame of reference in the atomic sphere around an atom at position $\mathbf{R}$. Inserting Eq. (2) to Eq. (4) leads to the following expressions for the angles $\varphi_{\mathbf{R}}$ and $\vartheta_{\mathbf{R}}$:[15]

$$\tan\varphi_{\mathbf{R}} = -\frac{\mathrm{Im}\, q^{(G)}_{\mathbf{R}1,\mathbf{R}2}}{\mathrm{Re}\, q^{(G)}_{\mathbf{R}1,\mathbf{R}2}} \tag{5}$$

$$\tan\vartheta_{\mathbf{R}} = 2\frac{|q^{(G)}_{\mathbf{R}1,\mathbf{R}2}|}{q^{(G)}_{\mathbf{R}1,\mathbf{R}1} - q^{(G)}_{\mathbf{R}2,\mathbf{R}2}}, \tag{6}$$

which define the output distribution of magnetic moments. The partial densities of states $n^{(G)}_{\mathbf{R}L\alpha,\mathbf{R}L\beta}$ are subsequently transformed to the local frame of reference by means of an equation analogous to Eq. (4), and the new charge and spin densities, interaction potentials, and potential parameters are calculated for each atomic sphere. This procedure is repeated until self-consistency is attained, i.e., both magnitudes and directions of the magnetic moments are equal to their respective input values. Some calculations in this paper were performed with the fixed prescribed directions of magnetic moments. Although these calculations are not fully self-consistent, yet they provide the transverse components of magnetic moments from which the stability of a prescribed magnetic order can be concluded.

It is a common problem within ASA, that the electrostatic energy contribution from the charge density in the overlapping volumes in incorrect.[22] In order to reduce this contribution we adjust the Wigner-Seitz radii to make the atomic spheres neutral. Since the excess charge in the system with equal Wigner-Seitz radii is moderate (0.08 electron/Fe atom), the ratio of neutral sphere radii converged to about $r_{Fe}/r_{Mn}=0.98$, almost independent of the magnetic order.

The exchange-correlation functional in the scalar relativistic Schrödinger equation is due to von Barth and Hedin[23] as parametrized by Janak.[24] The calculations performed with generalized gradient corrections (GGC) to the exchange-correlation potential use the form proposed by Perdew and Wang.[25] The core atomic charge densities are treated fully relativistically. A minimal basis set is adopted, which includes $3d$, $4s$, and $4p$ orbitals. For the Brillouin-zone integration the Methfessel-Paxton[26] smearing method on a grid of $(20\times20\times20)$ special points was used, corresponding to 1000 k points in the irreducible Brillouin zone.

III. RESULTS AND DISCUSSION

A. Ordered γ-FeMn

The results presented here were obtained for the ordered γ-FeMn compound with AuCu-I structure and an experimental lattice constant extrapolated to zero temperature $a=3.6$ Å .[1] The magnetic anisotropy energy due to spin-orbit coupling was not considered, because for cubic crystals it is of the order of 1μRy/atom, which is far below energy differences obtained in this study. In Fig. 1 three collinear [(a)–(c)] and four noncollinear [(d)–(g)] spin configurations are illustrated, for which the computations with fixed directions of the magnetic moments were performed. The total energies and magnitudes of magnetic moments are summarized in Table I. As can be seen, among the chosen configurations the configuration (d) with AFM order on the Fe-Fe and Mn-Mn sublattices and a perpendicular orientation of Fe and Mn moments possesses the lowest energy. The configuration (e) with the magnetic moments along the $\langle 111\rangle$ directions, proposed on the basis of the neutron-diffraction data, has an excess energy of only 0.1 mRy/atom. On the other hand, an imposed ferromagnetic interaction between Mn moments

[configuration (c)] or perpendicular arrangement of Mn moments [configuration (f)] results in unfavorable high-energy states. These facts confirm the AFM character of the Mn-Mn interactions. In the configuration labeled (b) in Fig. 1 asymmetric antiparallel magnetic moments develop on Mn atoms. The Mn magnetic moments parallel to FM-coupled Fe moments decrease, while the moments in the opposite directions assume large values, indicating that the Mn-Fe magnetic interaction is of AFM nature. From the nonvanishing transverse components of the magnetic moments in the local frame of reference we find that the configurations (e) and (g) are unstable, i.e., the systems would be driven away from their states, if a rotation of the moments would be allowed. The results in parentheses in Table I refer to the values obtained by Fujii *et al.*[9] A good agreement in the relative energies is obvious, but our values of Fe (Mn) magnetic moments are systematically somewhat larger (smaller) than the cited values.

The next conclusion can be drawn from the comparison of the configurations (a) and (d). These two configurations differ only by the relative orientation of the moments on the Fe and Mn sublattices and may be transformed into each other by a global rotation of the moments in one of the sublattices. It is easy to show that a pairwise Heisenberg Hamiltonian of the localized atomic moments is unable to explain the energy difference 0.41 mRy/atom between the two configurations: Evidently, the Fe-Fe and Mn-Mn interactions are the same in both cases and the overall Fe-Mn interaction is canceled in configuration (a) by equal number of parallel and antiparallel moments of the opposite type in every shell, in configuration (d) the Fe-Mn interaction is zero because of orthogonality of Fe and Mn moments. Hence within a pairwise Heisenberg model the two configurations are energetically degenerate.

In Figs. 2(a)–(d) the variation of the total energy and magnetic moments during a transition from configuration (b) → (d), (a) → (d), (b) → (g), (c) → (g), respectively, is shown. In the pictogram illustrating the process of moment rotations in each panel the bold (thin) arrows represent Mn (Fe) moments. The most notable result presented in Fig. 2(d) is a deep minimum of the total energy which lies lower than the energy of all configurations (a)–(g) discussed above. Further, an energy difference of about 2.4 mRy/atom is observed when the Mn moments change their orientation from parallel to the energetically most favorable canted configuration [Fig. 2(d)], whereas when the Fe moments are rotated [Figs. 2(a)–(c)] this difference shrinks to 0.4 – 0.9 mRy/atom. Hence it can be concluded that the strength of the Mn-Mn exchange interaction is three to six times stronger than that between Fe moments.

Up to now all results were obtained from calculations with fixed directions of the magnetic moments. If this constraint is removed the ground state corresponding to the energy minimum in Fig. 2(d) and given in Table I as the configuration (h) is obtained. The Fe moments are aligned parallel to each other and the Mn moments on the neighboring sites make an angle of $2\varphi = 128°$ with the resulting global Mn magnetization antiparallel to the Fe moments. Under the simplifying assumption of dominant nearest-neighbor interactions (although the pairwise Heisenberg model was shown to be an oversimplification) the magnetic energy per atom reads

$$E = E_0 - 2J_{Fe-Fe} - 2J_{Mn-Mn}\cos 2\varphi + 8J_{Fe-Mn}\cos\varphi, \tag{7}$$

leading to a rough estimate for $J_{Fe-Mn} \approx 0.5\, J_{Mn-Mn}$. This means that the interaction between Fe and Mn magnetic moments is antiferromagnetic but smaller than that between Mn moments.

Because the energy differences in Table I are relatively small, different LSD functionals could influence the energetics of the system. This is known to happen, for example, in bulk fcc Fe, where the LSD approximation without and with gradient corrections to the exchange-correlation functional leads to various spin-spiral-density-wave ground states.[17] For this reason we repeated the calculations for all configurations treated previously in the LSD+GGC approximation. The results collected in Table I show that both the energy differences and magnetic moments are larger, but the sequence of the configurations by an energy remains the same. The ground-state configuration (h) obtained by a free rotation of magnetic moments has the same arrangement of the magnetic moments, the angle between two nearest Mn moments being $2\varphi = 129°$.

B. Disordered γ-FeMn

All known experimental facts about γ-FeMn alloys were obtained on substitutionally disordered samples, therefore it is important to discuss the effects of disorder. Previous *ab initio* calculations, in which the configurational averaging is achieved by a single-site CPA with one Fe and one Mn atom per unit cell, give either magnetic moments of $m_{Fe} = 1.64\mu_B$, $m_{Mn} = -1.04\mu_B$,[10] or small magnetic moments $m_{Fe} < 0.12\mu_B$, $m_{Mn} < 0.29\mu_B$.[11] In Ref. 10 also another solution corresponding to a paramagnetic disordered local moment (DLM) state was investigated. For this purpose the two-component alloy Fe_xMn_{1-x} was treated as four-component model $[Fe^{\uparrow}_{0.5}Fe^{\downarrow}_{0.5}]_x[Mn^{\uparrow}_{0.5}Mn^{\downarrow}_{0.5}]_{1-x}$. In the paramagnetic phase symmetry arguments require the same magnitudes and probabilities of up and down moments. In the DLM state amplitudes $|m_{Fe}| = 1.48\mu_B$ and $|m_{Mn}| = 0.97\mu_B$ of the magnetic moments were determined. Clearly, the solution with small magnetic moments obtained in a two-component CPA is related to the DLM state solution, but with no restriction on the sizes of the magnetic moments.

The CPA results can be compared with our results if the projections of magnetic moments on an axis along the total magnetization are computed. This leads to $m_{z,Fe} = 1.42\mu_B$, $m_{z,Mn} = -0.91\mu_B$ (LSD approximation), or $m_{z,Fe} = 1.60\mu_B$, $m_{z,Mn} = -1.02\mu_B$ (LSD+GGC approximation). The good agreement of our and the CPA values indicates that a conceivable spin structure in a disordered FeMn alloy could be one with more or less parallel Fe moments and canted Mn moments with transverse components distributed in a plane perpendicular to the average Fe moment, a configuration not dissimilar to a spin-flop phase of a uniaxial antiferromagnet in a magnetic field. However, the question can be raised whether the ferromagnetic Fe-Fe interaction, estimated to be rather weak, is able to sustain the Fe moments parallel to each other.

To check this conjecture we performed an unconstrained noncollinear calculation for a unit cell containing 108 sites (a $3\times3\times3$ fcc lattice) occupied randomly by Fe and Mn at-

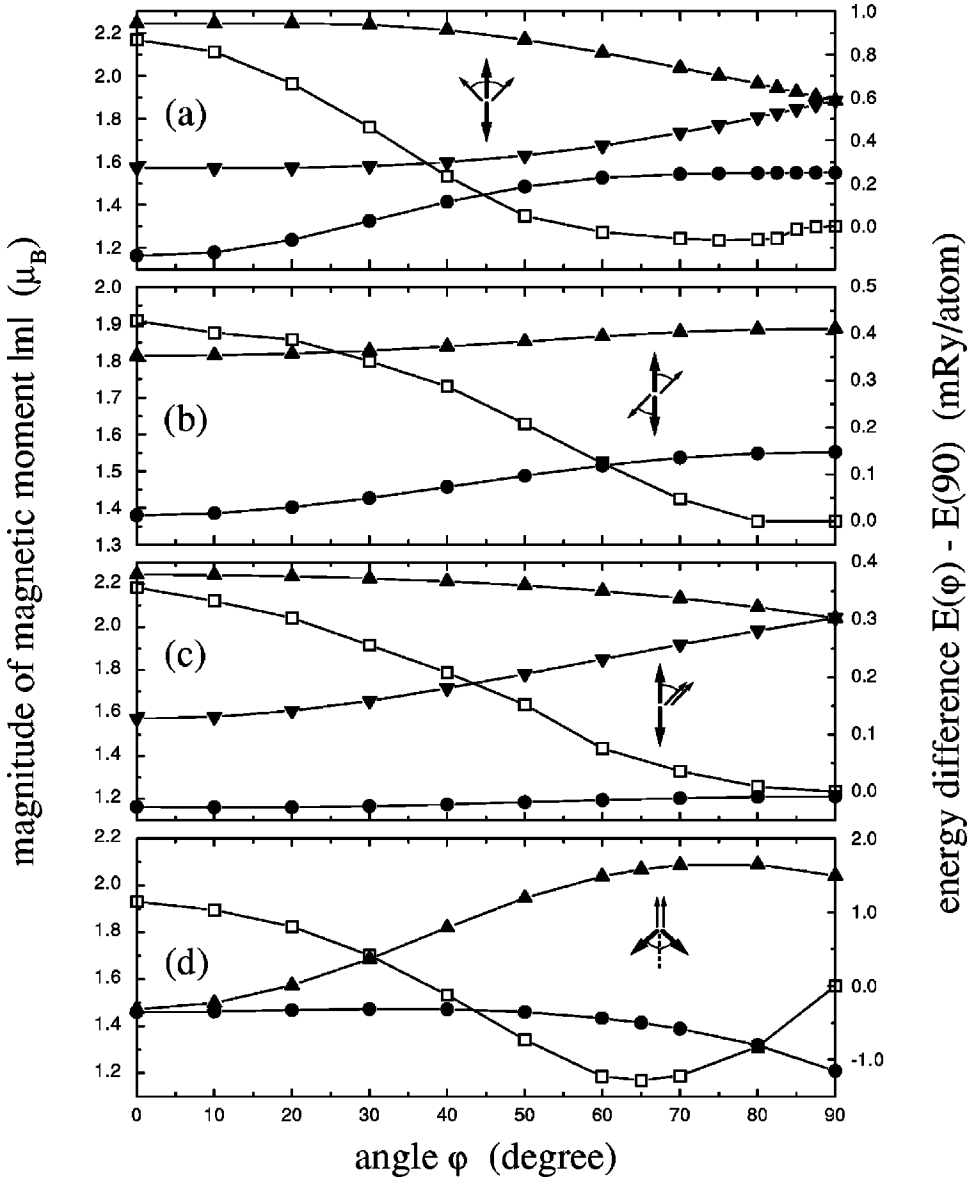

FIG. 2. Variation of the total energy and of magnetic moments as a function of the orientation of the magnetic moments on the Fe sublattice relative to the fixed direction of the Mn moments (a)–(c), and of the orientation of the Mn moments relative to a fixed direction of the Fe moments (d). Mn moments are represented by triangles, Fe moments by full dots (left-hand scale), energy differences by open squares (right-hand scale). In the pictograms defining the angle φ bold arrows represent the direction of the Mn moments, thin arrows those of Fe moments. Diagram (a) describes the transition of configuration (b) from Fig. 1 into configuration (d): transition from FM to AFM Fe-Fe coupling accompanied by a change from parallel to perpendicular Fe-Mn coupling. Diagram (b) describes the transition (a) → (d): global rotation of Fe moments, while maintaining AFM Fe-Fe coupling. Diagram (c) describes the transition (b) → (g): global rotation of Fe moments, while maintaining FM Fe-Fe coupling. Diagram (d) describes the transition (c) → (g): transformation from FM to AFM Mn-Mn coupling, accompanied by a change from parallel to perpendicular Fe-Mn coupling.

oms. The initial magnetic configuration was generated randomly and to every Fe (Mn) atom a small positive (negative) z component was added, in order to impose a global magnetization similar to the ground state of the ordered FeMn compound. In the k-space integration four k points were used. During the self-consistency cycle we observed after an initial stage with decreasing moments, a phase characterized by strong rotations of the magnetic moments leading to the formation of large magnetic moments distributed over a rather narrow interval and with almost exactly parallel and antiparallel orientations (see Fig. 3). The resulting magnetic structure is plotted in Fig. 4. The presence of disorder stabilizes nearly ideal collinear layered AFM structure of type I. The transverse components are smaller than $0.09\mu_B$. This result seems quite unexpected because usually a symmetry-breaking disorder in an antiferromagnet gives rise to more competing interactions and this leads to a magnetic structure with lower symmetry. Nevertheless, it was pointed out some time ago, that in many vector spin systems with competing exchange interactions nontrivial continuous degeneracies of the ground state may develop.[27] Quantitative predictions based on spin-wave analysis[28] and numerical simulations[29] were obtained for an XY square-lattice antiferromagnet with second-nearest-neighbor interactions. For $J_2 < -0.5|J_1|$ the

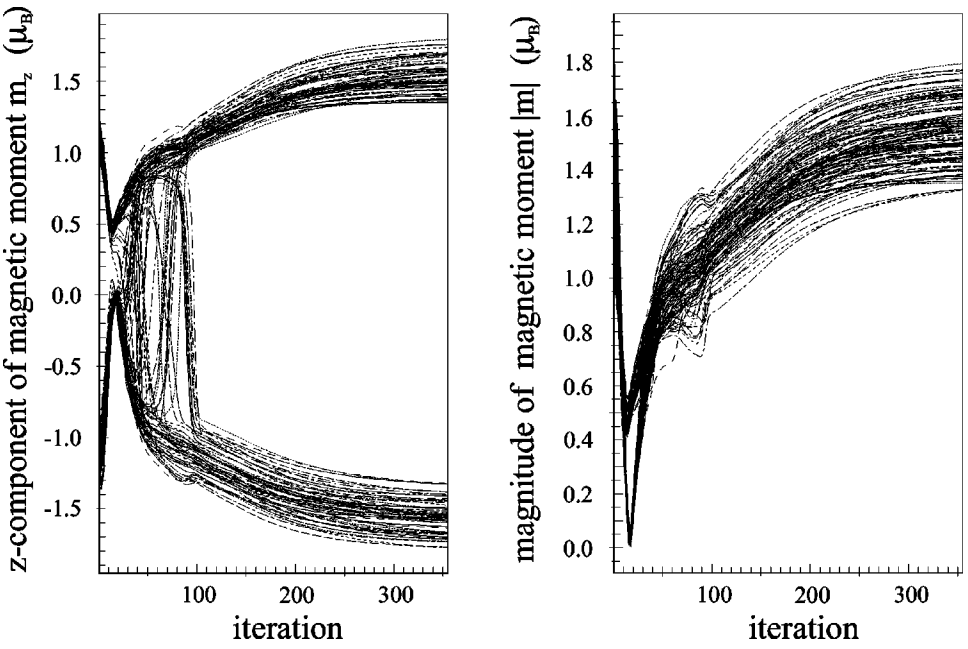

FIG. 3. Evolution of the z components and magnitudes of the local magnetic moments in a 108-atom supercell representing substitutionally disordered FeMn alloy during the self-consistent iterations (cf. text).

ground state breaks up into two decoupled penetrating square sublattices, each ordered antiferromagnetically. The fluctuations always present in real systems lift this degeneracy and they select specific magnetic states. It was found that thermal fluctuations favor collinear states whereas a dilution by nonmagnetic atoms selects noncollinear states. Because substitutional disorder produces random fields of a character similar to thermal fluctuations, a collinear state is preferred. The distribution of magnetic moments is shown in Fig. 5. The average magnitude of Fe magnetic moments is almost unchanged compared to the ordered γ-FeMn, $\langle|m_{Fe}|\rangle = 1.46\mu_B$, but that of the Mn moments decreases to $\langle|m_{Mn}|\rangle = 1.62\mu_B$. We believe the homogenization of the magnetic structure, i.e., the structure with nearly same magnetic moments on every site, resulting in quite isotropic magnetic interactions is substantial for producing a highly symmetric AFM ground state in a disordered γ-FeMn alloy.

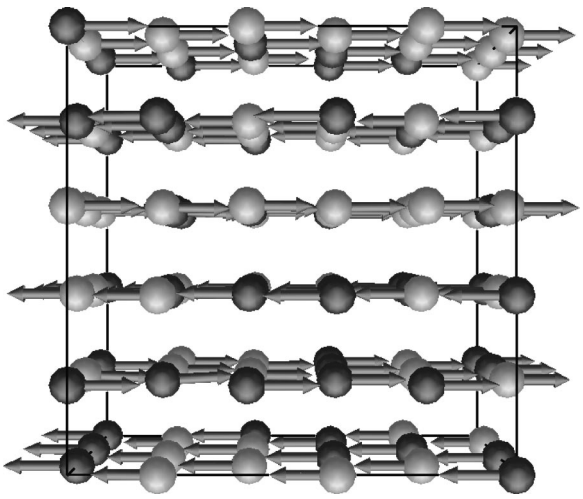

FIG. 4. The ground-state magnetic structure obtained in a unit cell with 108 atoms. Bright spheres represent Fe atoms, the dark spheres denote Mn sites.

IV. CONCLUSIONS

This paper presents a thorough analysis of magnetic structures in ordered and disordered γ-FeMn alloys using first-principle total-energy calculations and allowing for a noncollinear magnetic structure. In contrast to previous theoretical results for an ordered compound, which discerned only between a few highly symmetric spin configurations such as AFM type-I order or a noncollinear arrangement with moments along $\langle 111\rangle$ directions, we found a completely different ground-state solution with parallel Fe moments and the Mn moments tilted in opposite direction by 64° with respect to the direction opposite to the Fe moments. Within a model of localized moments, we estimated the Mn-Mn interaction to be antiferromagnetic and the strongest one in γ-FeMn. The Mn-Fe magnetic interaction is weaker and still of antiferromagnetic character, the ferromagnetic Fe-Fe coupling

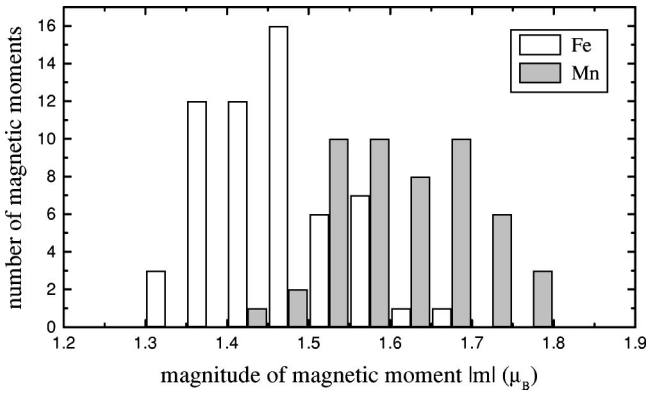

FIG. 5. The histograms present the distribution of Fe and Mn magnetic moments in a model of 108 atoms.

representing the weakest pair interaction. Besides, we concluded that a traditional pairwise Heisenberg Hamiltonian does not lead to a correct description of the magnetic order. Hence either many-body interactions must be considered or a vector model of localized moments is inappropriate for γ-FeMn.

If the disordered nature of γ-FeMn is taken into account, a collinear AFM type-I magnetic arrangement with nearly equal magnetic moments on Fe and Mn atoms was determined. These results are in accordance with one of the experimentally suggested ground states and with the observations that the broadening of the magnetic diffraction peaks typical for random alloys is missing. We note that the magnetic state of the disordered system cannot at all be inferred from the knowledge of the magnetic structure of its ordered counterpart, at least not for the system studied here. It is argued that the ordering of magnetic structure is driven by the random substitutional disorder in the alloy composition, a phenomenon known as ordering due to disorder.

ACKNOWLEDGMENTS

This work has been supported by the Austrian Ministry for Science and Transport within the project ''Magnetism on the nanometer scale '' and through the Center for Computational Materials Science.

[1] J. S. Kouvel and J. S. Kasper, J. Phys. Chem. Solids **24**, 529 (1963).
[2] Y. Endoh and Y. Ishikawa, J. Phys. Soc. Jpn. **30**, 1614 (1971).
[3] Y. Ishikawa and Y. Endoh, J. Appl. Phys. **39**, 1318 (1968).
[4] H. Umebayashi and Y. Ishikawa, J. Phys. Soc. Jpn. **21**, 1281 (1966).
[5] P. Bisanti, G. Mazzone, and F. Sacchetti, J. Phys. F: Met. Phys. **17**, 1425 (1987).
[6] K. Tajima, Y. Ishikawa, Y. Endoh, and Y. Noda, J. Phys. Soc. Jpn. **41**, 1195 (1976).
[7] M. Podgórny, Phys. Rev. B **45**, 797 (1992).
[8] J. Kübler, K.-H. Höck, J. Sticht, and A. R. Williams, J. Appl. Phys. **63**, 3482 (1988).
[9] S. Fujii, S. Ishida, and S. Asano, J. Phys. Soc. Jpn. **60**, 4300 (1991).
[10] D. D. Johnson, F. J. Pinski, and G. M. Stocks, J. Appl. Phys. **63**, 3490 (1988).
[11] N. I. Kulikov and C. Demangeat, Phys. Rev. B **55**, 3533 (1997).
[12] E. G. Moroni, G. Kresse, J. Furthmüller, and J. Hafner, Phys. Rev. B **56**, 15 629 (1997).
[13] T. Asada and K. Terakura, Phys. Rev. B **47**, 15 992 (1993).
[14] M. Eder, J. Hafner, and E. G. Moroni, Surf. Sci. Lett. **243**, L244 (1999); Phys. Rev. B **61**, 11 492 (2000).
[15] J. Sticht, K.-H. Höck, and J. Kübler, J. Phys.: Condens. Matter **1**, 8155 (1989).
[16] O. N. Mryasov, A. I. Liechtenstein, L. M. Sandratskii, and V. A. Gubanov, J. Phys.: Condens. Matter **3**, 7683 (1991).
[17] M. Körling and J. Ergon, Phys. Rev. B **54**, R8293 (1996).
[18] V. P. Antropov, M. I. Katsnelson, B. N. Harmon, M. van Schilfgaarde, and D. Kusnezov, Phys. Rev. B **54**, 1019 (1996).
[19] T. Oda, A. Pasquarello, and R. Car, Phys. Rev. Lett. **80**, 3622 (1998).
[20] O. K. Andersen and O. Jepsen, Phys. Rev. Lett. **53**, 2571 (1984).
[21] O. K. Andersen, O. Jepsen, and D. Glötzel, in *Highlights of Condensed-Matter Theory*, edited by F. Bassani, F. Fumi, and M.P. Tosi (North-Holland, New York, 1985), p. 59.
[22] X.-G. Zhang and D. M. C. Nicholson, Phys. Rev. B **60**, 4551 (1999).
[23] U. von Barth and L. Hedin, J. Phys. C **5**, 1629 (1971).
[24] J. F. Janak, Solid State Commun. **5**, 53 (1978).
[25] J. P. Perdew and Y. Wang, Phys. Rev. B **45**, 13 244 (1992).
[26] M. Methfessel and A. T. Paxton, Phys. Rev. B **40**, 3616 (1989).
[27] J. Villain, Z. Phys. B **33**, 31 (1979).
[28] Ch. Henley, Phys. Rev. Lett. **62**, 2056 (1989).
[29] D. Spišák, IEEE Trans. Magn. **30**, 1081 (1994).